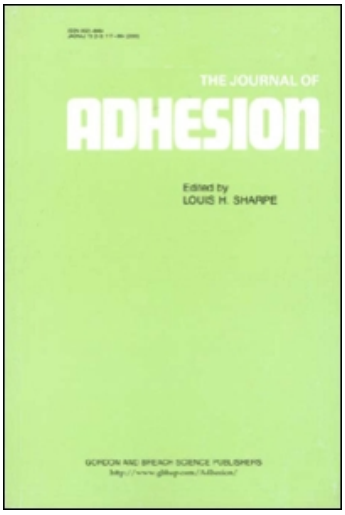

The Journal of Adhesion
Publication details, including instructions for authors and subscription information:
http://www.informaworld.com/smpp/title~content=t713453635

A Unified Approach for Predicting the Strength of Cracked and Non-Cracked Adhesive Joints

A. D. Crocombe[a]; G. Richardson[a]; P. A. Smith[b]
[a] Department of Mechanical Engineering, [b] Department of Materials Science and Engineering, University of Surrey, Guildford, Surrey, UK

To cite this Article Crocombe, A. D. , Richardson, G. and Smith, P. A.(1995) 'A Unified Approach for Predicting the Strength of Cracked and Non-Cracked Adhesive Joints', The Journal of Adhesion, 49: 3, 211 — 244
To link to this Article: DOI: 10.1080/00218469508014357
URL: http://dx.doi.org/10.1080/00218469508014357

J. Adhesion, 1995, Vol. 49, pp. 211–244
Reprints available directly from the publisher
Photocopying permitted by license only

A Unified Approach for Predicting the Strength of Cracked and Non-Cracked Adhesive Joints*

A. D. CROCOMBE and G. RICHARDSON

Department of Mechanical Engineering

P. A. SMITH

Department of Materials Science and Engineering, University of Surrey, Guildford, Surrey, GU2 5XH, UK

(Received May 23, 1994; in final form September 6, 1994)

This paper presents an investigation of suitable failure criteria for predicting the strengths of uncracked and interfacially-cracked adhesively-bonded joints. A detailed experimental study of both bulk adhesive and adhesive joint behaviour has been carried out. The effect of both strain rate and temperature on the response of the adhesive to mechanical loading has been investigated through a series of tensile tests. The resulting data were used to construct an empirical model for the behaviour of the adhesive. A novel test method based on a four-point bend specimen has been used to investigate how the hydrostatic stress affects the response of the adhesive. Extensive tests on adhesive joints, subjected to different modes of loading and different lengths of interfacial cracks, have provided comprehensive joint strength data and insight into the site and locus of joint failure initiation. Following this, various failure criteria have been evaluated by carrying out detailed linear elastic and non-linear elasto-plastic two-dimensional analyses of the joints tested. Three-dimensional analyses provided modified loads for these two-dimensional analyses that more accurately reproduce the conditions on the plane of failure. Criteria based on critical stress or strain components at a distance from the point of singularity were investigated. A procedure for accounting for the strain rate effects of the adhesive has been incorporated with the non-linear analyses. Criteria based on critical energy release rates have been evaluated from the linear elastic analyses of the joints with interfacial cracks diminishing to very small sizes. Finally, non-linear springs along a plane of failure have been used to model a line of localised damage, resulting in joint failure criteria based on a critical opening displacement. This last method provides the most physically acceptable way of predicting the strength of cracked and non-cracked joints using the same failure criterion.

KEY WORDS: adhesive joint failure; rate dependent behaviour; process zone; softening springs; mixed mode interfacial failure; failure criteria

1. INTRODUCTION

Structural adhesives provide a viable alternative to the more traditional joining techniques such as welding, bolting, etc. The recent toughened adhesives have excep-

* Part of this paper were presented at Adhesion '93, the Fifth International Conference of the Adhesives Section of the Polymer Industry Division of The Institute of Materials, held at The University of York, York, UK, September 6–8, 1993.

tional mechanical properties. However, in many instances, they are not being used to their full potential because it is not possible to predict the strengths of bonded components reliably. This need has been recognised in a number of recent review documents.[1,2] Numerous criteria have been used for predicting bonded joint strength. These include criteria based on maximum values of stress or strain,[3,4] limit state concepts,[5] characterising the singular stress field present at a non-cracked bi-material terminus,[6-8] use of linear elastic fracture mechanics (LEFM) concepts both along the interface and within the adhesive[9,10] and use of damage and ductile fracture mechanics concepts.[11,12]

Each of the above criteria are not without their problems and limitations. Criteria based on stress and strain often use data that have been obtained from an analysis that includes a singular stress or strain field. Thus, it is necessary to use values that are averaged over, or evaluated at, some arbitrary distance from the singular point. A limit state analysis usually only applies to shear-loaded, ductile adhesive joints. Non-cracked bi-material parameters are often specific to a particular range of joint configurations. The principles of LEFM can only be applied to joints with macro-sized cracks and, thus, are not applicable to adhesive joints that are at beginning their service life and so do not contain cracks of such a size. To overcome this, damage mechanics principles are being employed but this is a concept still in its infancy.

Thus, none of these criteria are entirely satisfactory and this work has been carried out to investigate further the application of many of them, including stress and strain and LEFM-based criteria as well as a new criterion which models damage as being localised on a line ahead of the singular point. This last criterion is somewhat akin to the Dugdale model of ductile fracture.[13] We are primarily concerned with the strength of joints that are notionally uncracked. However, it is recognised that even non-cracked joints theoretically contain a bi-material singularity. As joint failure occurs the governing singularity changes from that defined by a bi-material condition to the stronger singularity governed by the crack, postulated to be interfacial initially. Thus, it was thought to be instructive to study, experimentally and numerically, the effect of a decreasingly small interfacial crack in an adhesive joint.

In order to investigate the relevance of the failure criteria above, and to consider other possible approaches, it is necessary to have high-quality experimental data, defining not only the response of the joints but also of the constituent parts. Adhesives, and the joints which utilise them, are rate and temperature sensitive. It is important to be able to characterise their behaviour accordingly and to carry out experiments under carefully controlled conditions. There are a number of other parameters (such as cure and post cure conditions, surface preparation, manufacturing technique, etc.) that might also significantly change the response of a joint and so need to be carefully controlled. In order to obtain a comprehensive set of data, in the present study more than seventy joint tests and twenty tests on specimens of the bulk adhesive have been carried out. To assess the effectiveness of any failure criterion it is necessary to apply it to different configurations of adhesive joint. This has been done by subjecting the joint to two different modes of loading, typical of the loading experienced in peel and lap shear joints. These two modes, along with interfacial crack length, form the parameters of the joint tests. Bulk adhesive specimens have been subjected to tensile and four-point bend tests. The former has been used to determine both rate and temperature

dependent constitutive behaviour of the adhesive. The bend tests provide additional tensile behavior but also give the adhesive's response in compression. From the tensile and compressive behaviour the ratio of flow stress in compression to tension can be determined. This is the parameter that controls the hydrostatic sensitivity of the material and is required for the non-linear analytical work.

The initial finite element analyses assumed linear elastic behaviour and were very detailed, with element sizes of less than 1 nm at the point of singularity. These analyses enabled the singular stress fields to be studied in detail and offered insight into the transition from an uncracked to a micro-cracked configuration. The stress fields and energy release rates have been found for unit loads. These can be scaled to determine the conditions at the point of failure and used to find the optimum linear elastic failure criteria parameters. By allowing the adhesive to become perfectly plastic the stress (but not the strain) singularity disappears and the problem becomes non-linear. Thus, it is not possible to scale the results and multiple analyses for each configuration are required to enable the optimum elasto-plastic failure criteria parameters to be evaluated. Further, it was necessary to determine the effective strain rate so that appropriate material properties could be used. These strain rates were calculated using experimental loading rate data in conjuction with the non-linear strains from the elasto-plastic finite element analyses. Finally, analyses which allow localised damage to occur along the interface ahead of the singularity have been carried out. Non-linear springs have been used for this work which has been termed "stress-controlled separation". The effect of separation at both a constant stress (perfectly plastic) and reducing stress (softening) have been considered.

The subsequent sections present separate experimental procedures, results and discussions for the joint and bulk tests. This is followed by details of, and results from, the linear elastic, elasto-plastic and stress-controlled separation analyses which are also presented in separate sections. Each of the results sections contains its own discussion.

2. ADHESIVE JOINT TESTS

2.1 Manufacturing Procedure

The test specimen, based on the ASTM D1062–78 cleavage specimen, is shown, together with the loading rig, in Figure 1. The rig provides a means of subjecting the joint to a range of loading modes. In this work, the loading from the fork was applied either normal to, or at 45° to, the adhesive layer. These shall be referred to as mode I and mixed mode loading, respectively. Such terminology is only notional because the asymmetry caused by the interfacial crack and dissimilar materials will generate some mixed mode loading even in the "mode I" configuration. An adhesive layer thickness of 2 mm (larger than that normally found in practice) was used to enable an accurate overlap end geometry to be obtained. The adhesive used was a two-part, cold cured, unfilled epoxy having a sufficiently low viscosity (1000 cP) to enable the specimens to be cast. The adherends, made from high strength aluminium (2014–T3) were abraded with 600 grade silicon carbide paper to give a consistent morphology, ultrasonically cleaned in a detergent solution, rinsed and then given a chromic acid etch (UK MOD DTD 915B). Interfacial cracks were introduced using PTFE (polytetrafluoroethy-

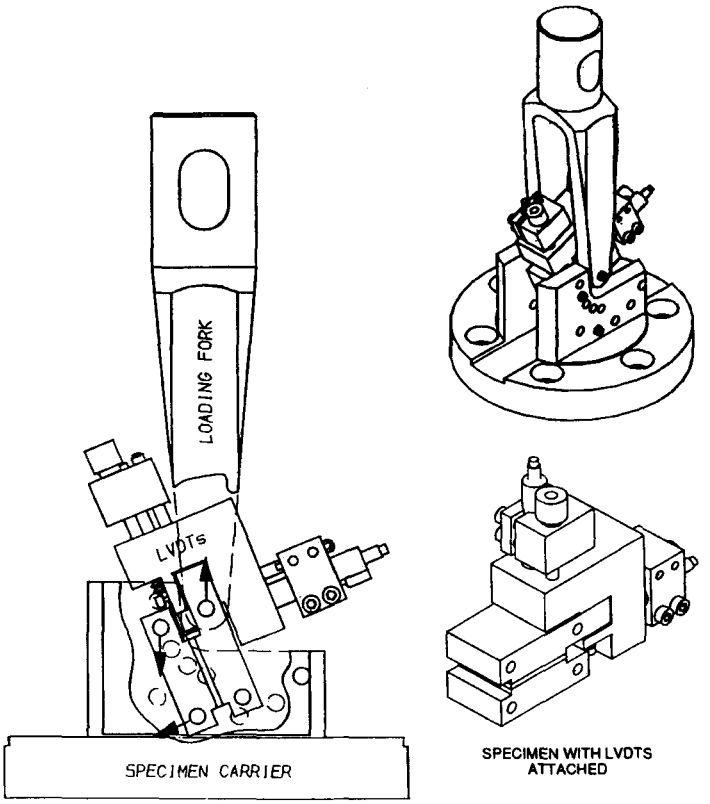

FIGURE 1 Detail of the adhesive joint and the loading rig.

lene) tape compressed onto the surface of the upper adherend by careful rolling with a clean glass rod. Small crack lengths (< 1 mm) were obtained by using oversized adherends which were machined to size after manufacture. The same procedure was used to produce a well-defined end geometry for the uncracked joints. The adherends were located in a jig which separated them by the required adhesive thickness. A self-adhesive glass fiber tape with an inner strip of PTFE tape was wrapped around the substrates to form a mould into which the adhesive is injected. To ensure consistency of cure, the joints were always left cure at 30 °C for 48 hours, then stored in a desiccator for at least ten days after which they were post cured at 60 °C for 6 hours. All specimens were left in a desiccator for at least two further weeks before testing. Generally, excellent void-free specimens were obtained from the above procedure. For each mode of loading three classes of specimen were tested; uncracked, short cracks (0–1 mm) and long cracks (1–3 mm). Twelve specimens were tested in each class, giving a total of 72 tests. The specimens were manufactured in batches of twelve. To assess batch-to-batch variation, each manufacturing batch provided two specimens to each of the six classes of specimen.

2.2 Test Procedure

The joint specimens were loaded to failure using the loading rig shown in Figure 1 attached to a 100 kN Instron 6025 testing machine. There are two features of particular

interest. Firstly, the use of a tapered loading pin in the upper adherend eliminated any angular misalignment between the loading holes in front of the upper and lower adherends produced during specimen manufacture. Horizontal movement of the tapered pin ensured that the loading between the pin and hole was applied equally on both sides of the adherend. Secondly, LVDT's were mounted on the extended front portion of the upper adherends. These were used to measure the separation and sliding between the upper and lower adherends, referred to as mode I and mode II displacements, respectively. A constant crosshead speed of 0.05 mm min^{-1} was used for all tests and load, time and mode I and II displacements were recorded on an Apple Macintosh computer using a data-logging programme written using LabView.

2.3 Result and discussion

The specimens were loaded to failure which generally occurred catastrophically. The load-displacement curve did not show the sudden increase in compliance that would be expected if substantial yielding occured. From the data recorded and the observations, made, results were obtained for the following: failure loads, loading rates, compliances, failure initiation site and locus of failure.

Considering first the failure loads, there was considerable scatter in the data despite the care that was taken in the manufacturing and testing procedures. However, when the failure load for each specimen was normalised with respect to the average mode I uncracked failure load for their own manufacturing batch the results are much more consistent and these are presented later in Figures 13,18 and 23, where it can be seen that the loads decrease gradually with increasing crack length. The average uncracked failure load for both modes of loading are given in Table I. In this and all subsequent tables, the bracketed value refers to the standard deviation of the data. Using these data in conjuction with Figures 13,18 and 23 it can be seen that the strength of a specimen is higher when it is subject to a mixed mode rather than a mode I load. It should also be noted that there is no sudden change in strength between uncracked and short cracked specimens.

Next, we consider the rate of loading experienced by the joints. This is important because, as will be seen in the next section, the adhesive is significantly rate dependent, Such behaviour needs to be accounted for in the stress analysis of these joints. From the load-time response, the gradient of which tends to increase slowly up to the point of sudden failure, it is possible to obtain an approximate rate of loading for each of the joints tested. This is shown in Figure 2 for all mode I joints, where it can be seen that the rate of loading is relatively insensitive to the crack length. A similar variation, but at a higher rate, is also found for the mixed mode joints. The average rates of loading used for all mode I joints and all mixed mode joints is summarised in Table II.

TABLE I
Average uncracked failure loads

Mode of loading	Failure load/N
Mode I	1436(188)
Mixed mode	2269(246)

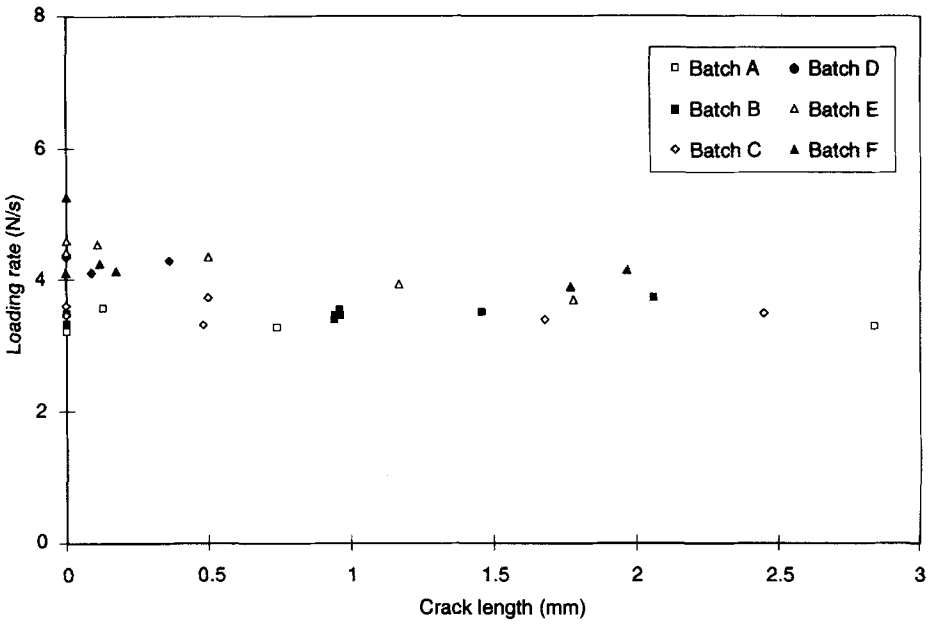

FIGURE 2 Variation of loading rate with crack length for all mode I joints.

Table III shows the average ratio of mode I to II (opening to shear) displacement (measured by the lVDT's shown in Fig. 1) at beginning of a test for both mode I and mixed mode loadings. The mixed mode loading is dominated by the shear (mode II) displacement.

A visual inspection of the failed surfaces revealed a site of failure initiation in many of the specimens at some discrete point along the crack tip/singularity. Some specimens showed two distinct failure initiation sites. To determine the preferred region of initiation for each mode of loading, histograms were plotted from the available data. Figure 3 shows histograms illustrating the variation of the location of the site of failure initiation with distance from the centre of the joints. It can be seen that for the mode I joints the

TABLE II
Average loading rates for the joints tested

Loading mode	Mode I	Mixed mode
Loading rate (N/s)	3.84 (0.48)	4.45 (0.51)

TABLE III
Average mode I : II displacement ratio for uncracked joints

	Mode I	Mixed mode
Displacement ratio	1.038 (0.179)	0.238 (0.028)

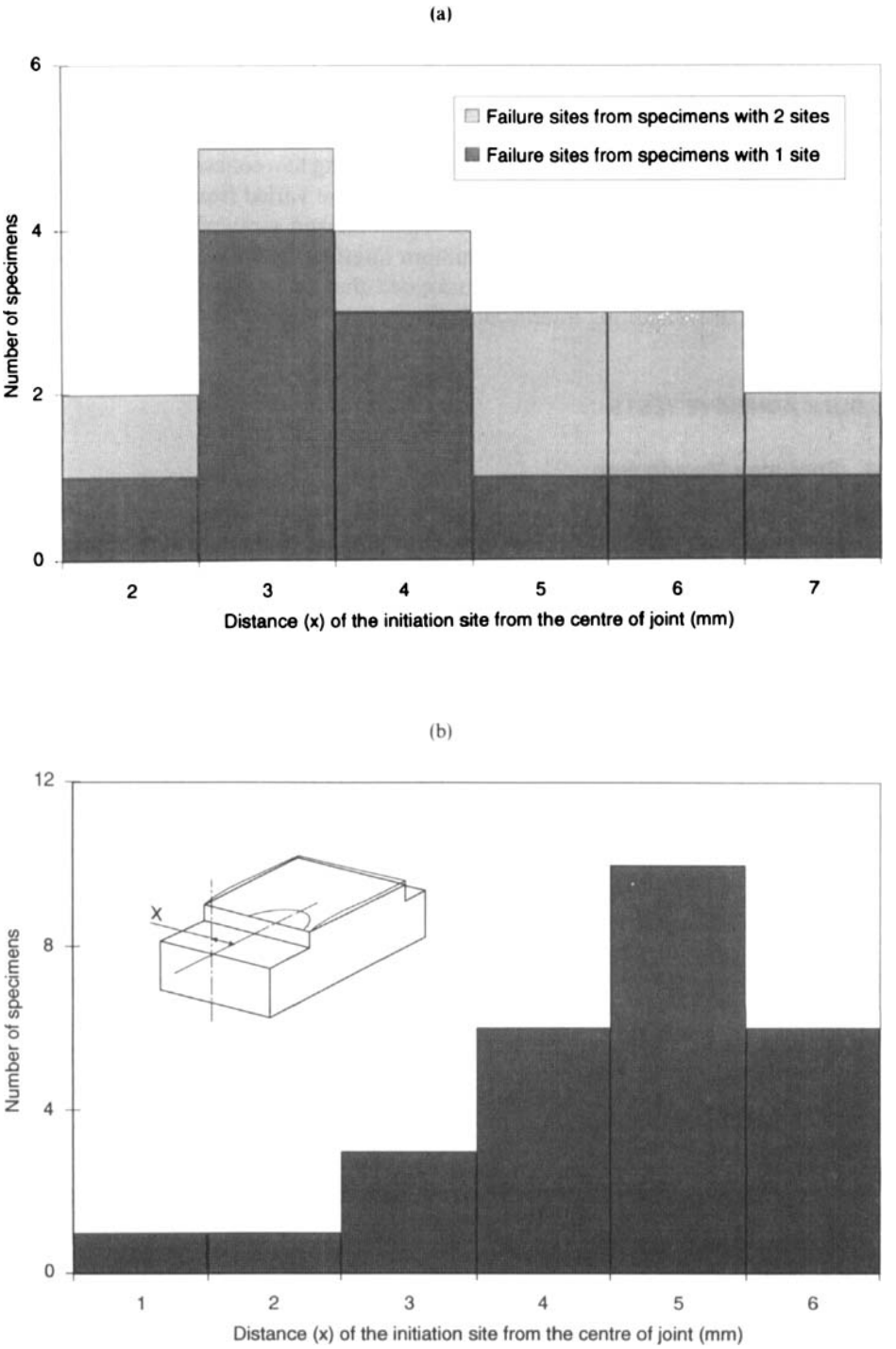

FIGURE 3 Histograms for failure initiation sites in a) mode I and b) mixed mode joints.

preferred site of failure is about 3 mm from the centre while for mixed mode joints it is at 5 mm from the centre. Further, some of the mode I specimens had two distinct failure sites. The site of failure initiation appears to correspond with the position of maximum stress and energy release rate, the variation of which, across the front of the joint, has been shown[17] to be a maximum over the middle region, reducing at the joint edges. The failure always appeared to occur interfacially initially, changing to a cohesive mode as the crack propagated. However, the amount of interfacial failure varied from specimen to specimen. In order to investigate the interfacial region further, x-ray photelectron spectroscopy (XPS) was carried out on the aluminium interface in the interfacial region, after failure. The absence of a nitrogen peak indicated that no adhesive was present on the failure surface, thus sugesting interfacial failure.

3. BULK ADHESIVE TESTS

3.1 Specimen Manufacture

It was necessary to obtain full elasto-plastic, rate-dependent adhesive constitutive data for the various analyses that are to be carried out. The necessary data were obtained from specimens of bulk adhesive that were tested both under tension (to determine rate and temperature sensitivity of the adhesive uniaxial properties) and in four-point bending (to ascertain the ratio of the plastic flow stress in compression to that in tension, S). Details of the specimens used for these tests can be seen in Figure 4. They were both manufactured in the same way, cast in a closed mould. Before assembling the moulds, the side pieces

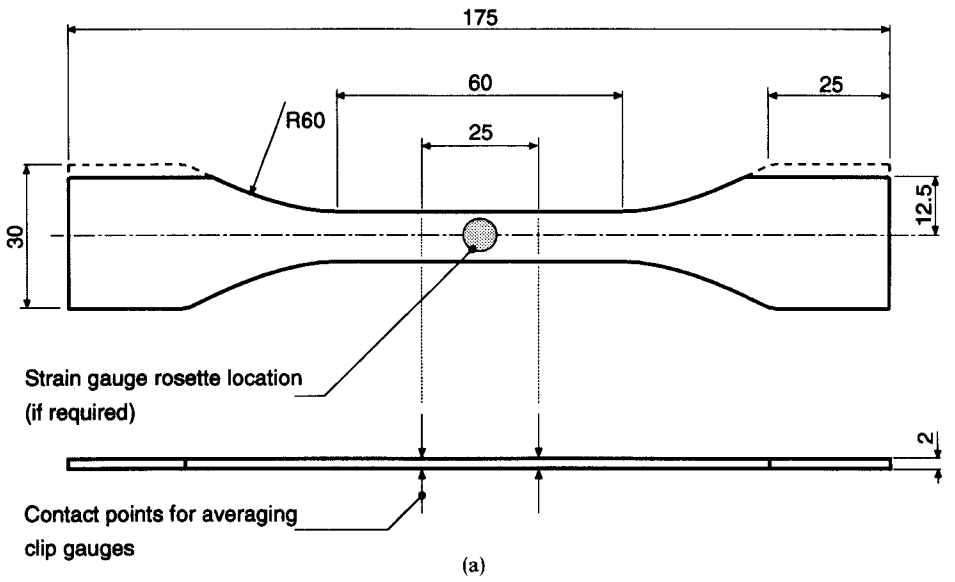

Note:- (i) All dimensions in millimetres. (ii) Dashed regions were removed after casting.

FIGURE 4 Bulk adhesive: a) tensile and b) bend test specimens.

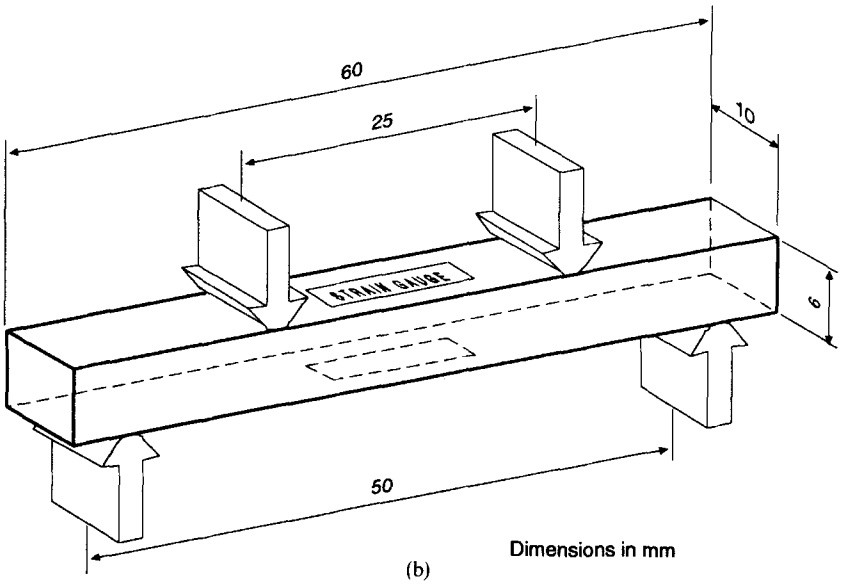

FIGURE 4 *(Continued.)*

were sprayed with PTFE spray and a thin polyimide film was attached to the inner faces of the top and bottom plates using a thin layer of silicone adhesive. The adhesive was prepared and cured in exactly the same way as outlined in the section above on adhesive joint manufacture.

Strain guages were used on some of the tensile specimens to determine Poisson's ratio and on all the bend specimens. The gauges were bonded with the recommended cyanoacrylate adhesive and the terminal tags were fixed with a more flexible silicone adhesive. When the terminal tags were bonded using the cyanoacrylate it was found that they caused premature failure.

3.2 Test procedures

3.2.1 Tensile tests The tests investigating the effect of rate on the mechanical response of the adhesive were carried out on an Instron 6025 (a servo-mechanical machine) where temperature control was not possible. In order to assess the effect of temperature variation, subsequent tests were carried out on an Instron 1341 (a servo-hydraulic machine) at two controlled temperatures, 15°C and 25°C.

On all the tests the specimen strain was measured using clip-on extensometers. The signal from these extensometers was also used to control the strain rate of the test by adjusting the cross-head speed in closed loop control. Three strain rates were considered, namely 0.02% min,$^{-1}$ 1% min^{-1} and 50% min.$^{-1}$ It can be seen by reference to Table VIII in a later section that this range of strain rates includes the strain rates experienced by the adhesive during the joint tests. During testing load, strain and time were recorded on a Macintosh computer using a custom-designed, data-logging system. At least three specimens were tested at each strain rate and temperature under consideration.

Specimens for the same tests were selected from diffferent batches to assess any variation introduced during manufacturing. However, as will be seen, the consistency of the results was excellent and no such variation was noted.

3.2.2 Bending tests These were carried out to measure the ratio of flow stress in compression to tension and this is achieved by measuring the strains corresponding to the applied load on the upper and lower surfaces at the centre span of a four-point bend specimen. The theoretical derivations for this test and the procedure for converting the surface strain-applied load data to tensile and compressive stress strain curves has been discussed elsewhere.[14] Tests were carried out on the Instron 6025. The specimen is placed on the outer anvils of the test rig which are mounted on the moving crosshead of the Instron. The strain gauges are connected, using 3-wire, quarter-bridge circuitry, to a strain gauge amplifer. The output from this, together with the load from the Instron, is directed to the same data-logging program used for the rest of the tests. The crosshead is then driven at a constant speed of 0.1 mm min^{-1} bringing the specimen into contact with the inner anvils fixed on the load cell of the machine. When the surface strains reach 5%, the limit of the strain gauges, the test is halted.

3.3 Results and Discussion

3.3.1 Tensile tests All the resulting tensile stress-strain curves are shown in Figure 5. The data are so consistent that in places it is difficult to see the symbols representing the

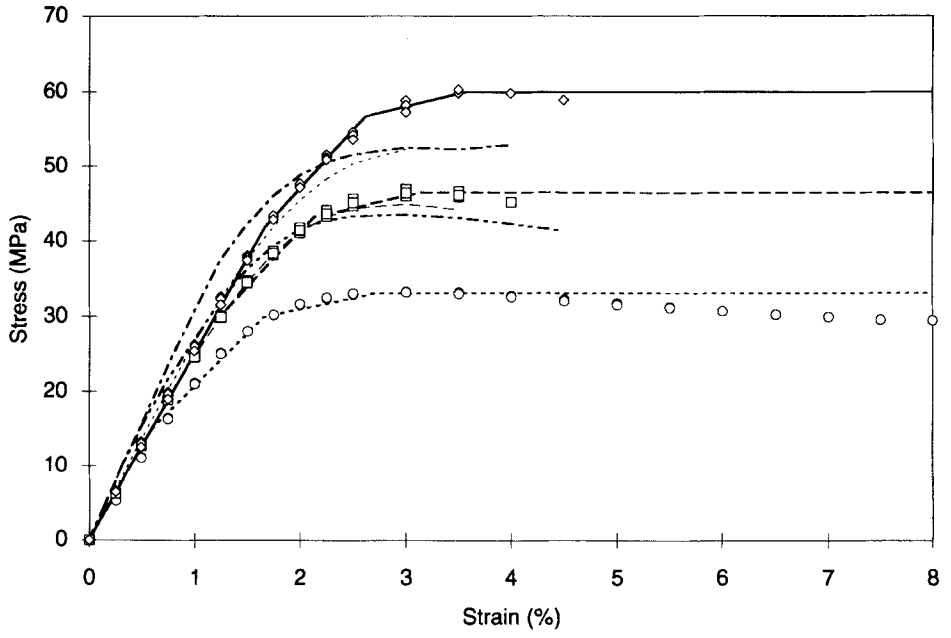

FIGURE 5 Tensile and compressive stress strain data and an empirical model for the bulk adhesive. (50%/min◇, 50%/min model——, 1%/min □, 1%/min model– – –, 0.02%/min○, 0.02%/min model - - - -, 1%/min15 °C - - - -, 1%/min 25 °C – –, 4 point bend tension ----- 4 point bend compression – – – –). All data are experimental and evaluated at 20 °C unless otherwise specified.

separate tests. For clarity, the key material data from the tests at room temperature are summarised in Table IV. As expected, as the rate of straining increases so does the level of stress that the material can withstand. It would appear that there is a logarithmic dependence of the post-yield stress on the strain rate. This is in keeping with Eyring's viscous flow model.[15] The data obtained at room temperature was notionally at 23 °C and it can be seen, Figure 5, that this is consistent with the data obtained from tests at 15 °C and 25 °C which clearly show that post-yield stresses decrease with temperature, as expected. As well as obtaining uniaxial tensile data, these tests have also given Poisson's ratio for the adhesive. Figure 6 shows how the measured Poisson's ratio varies with longitudinal strain. It can be seen that it is effectively constant and a value of 0.395 has been found by using linear regression on the data.

An empirical model has been developed which describes the rate-dependent behaviour of the adhesive. The response from this model is shown in Figure 5 where it can be seen

TABLE IV
Summary of tensile rate dependent data for the bulk adhesive

Strain rate (%/min)	Modulus (MPa)	Ult. stress (MPa)	Strain at ult. stress %
0.02	2140(1)	33.2(0.0)	2.86(0.07)
1.0	2520(7)	46.6(0.5)	3.07(0.05)
50.0	2580(48)	59.3(1.0)	3.43(0.28)

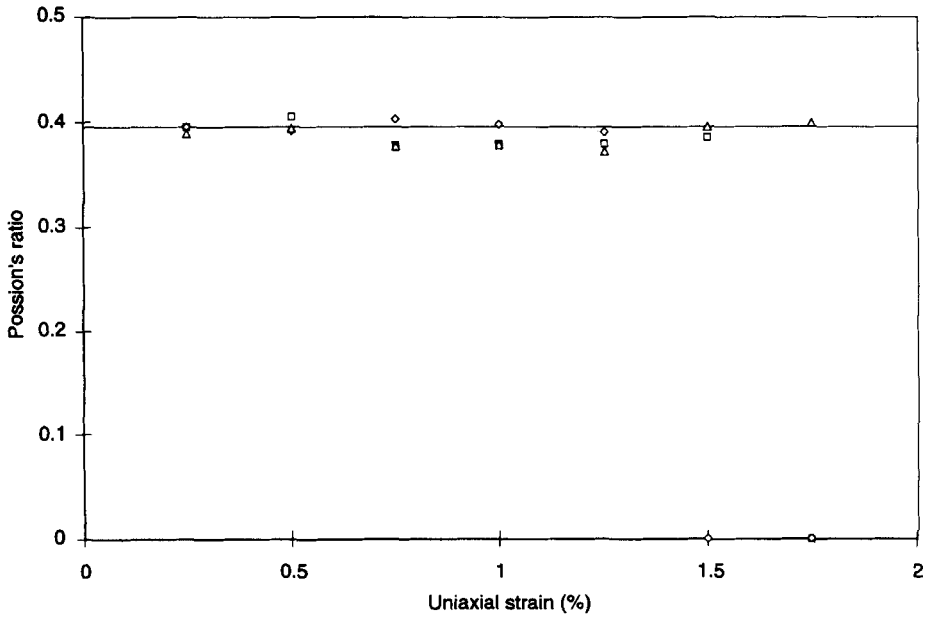

FIGURE 6 Variation of Poisson's ratio with longitudinal strain.

that it is a very good fit to the measured data. The empirical model was developed by considering three points on the stress-strain curves: the point of initial yield (σ_y, ε_y), the point of ultimate stress ($\sigma_u, \varepsilon_{\sigma u}$) and an intermediate point (σ_i, ε_i). This last point has no physical significance but, lying mid-way between the yield and ultimate strains, provides a multi-linear fit to the data. The other points have been determined "by eye" for each of the data sets. Table IV shows that the modulus increases with strain rate but in this model it has been assumed constant at 2500 MPa. Figure 5 shows that this does not significantly affect the fit to the experimental data. Taking the stress to be measured in MPa and the strain and strain rate to be in % and %/min, respectively, we begin with the observation already made that the ultimate stress varies logarithmically with the strain rate. Fitting this to the data yields

$$\sigma_u = 7.9 + 46.6 \log(\varepsilon') \tag{1}$$

Next, from Figure 5, it can be seen that the strain at the ultimate stress ($\varepsilon_{\sigma u}$) is essentially linear with the ultimate stress. This yields the following equation

$$\sigma_{\sigma u} = 0.032\, \sigma_u + 1.65 \tag{2}$$

Now, it would also appear that the departure from linearity, or yield stress σ_y, occurs at a fixed stress below the ultimate stress, giving

$$\sigma_y = \sigma_u - 18.0 \tag{3}$$

The strain at yield can be obtained from the Young's modulus, assumed constant here at 2500MPa. Now, only the intermediate stress and strain are required. The intermediate strain (ε_i) is taken as the average of the two other strains, thus

$$\varepsilon_i = (\varepsilon_{\sigma u} + \varepsilon_y)/2 \tag{4}$$

By a process of trial and error it was found that the intermediate stress, σ_i, can be expressed in terms of the other two stresses as

$$\sigma_i = \sigma_y + 0.82(\sigma_y + \sigma_u) \tag{5}$$

3.3.2 Four point bend tests The surface strain and load data are processed according to a specified procedure.[14] The resulting tensile and compresive stress-strain data are also shown in Figure 5. It can be seen that the tests produce reasonably consistent data, perticularly in comparison. The surface strain rate in this test is not constant but varies from 0.1 to 0.25%/min . It can be seen to be reasonably consistent with the data found from the tensile tests. The discrepancies occur because not only do the surface strain rates vary throughout the test but, at any given moment, the strain rate also varies across the specimen thickness. However, the response of the specimen is dominated by the material behaviour near the surfaces and thus the discrepancies are not as significant as might be anticipated. The data that is required, however, is the ratio of compressive to tensile flow stress(S) and this is shown plotted against plastic strain in Figure 7, assuming that the material follows a work hardening law. This distribution is hardly affected if strain

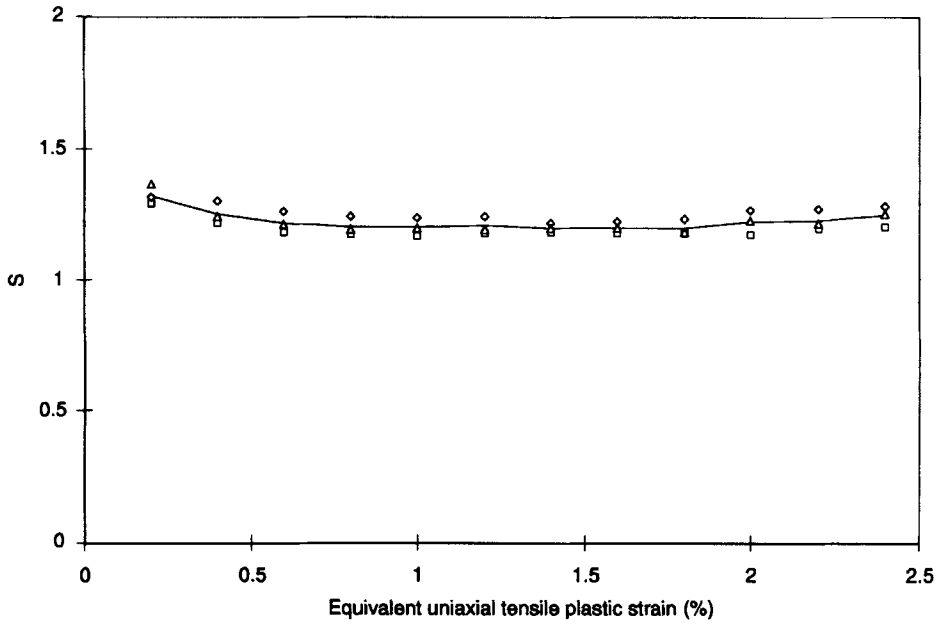

FIGURE 7 Variation of compressive to tensile flow stress assuming work hardening.

hardening is assumed. It can be seen that S varies about a value of 1.2 and this is the value that has been used in subsequent stress analyses of these joints discussed later.

4. DEVELOPMENT OF THE FINITE ELEMENT MODEL

In order to establish the appropriate degree of mesh refinement, finite element analyses were carried out on a point-loaded interface crack between two infinite half-planes and the results for energy release rates and stress fields were compared with the analytical solution.[16] The mesh used is shown in Figure 8. The parameters varied were the number of radial fans and the smallest element size. A comparison of the energy release rates for a selection of the analyses is shown in Table V. It can be seen that with radial zones of 22.5°

TABLE V
Summary of finite element assessment of refinement zones

Analysis	Radial zones in 90°	Smallest element size/crack size	Error in Energy Release Rate (%)
A	1	0.25	11.9
B	2	1×10^{-9}	4.9
C	4	1×10^{-9}	0.7
D	4	1×10^{-6}	0.6
E	4	1×10^{-3}	0.5
F	6	1×10^{-9}	0.4

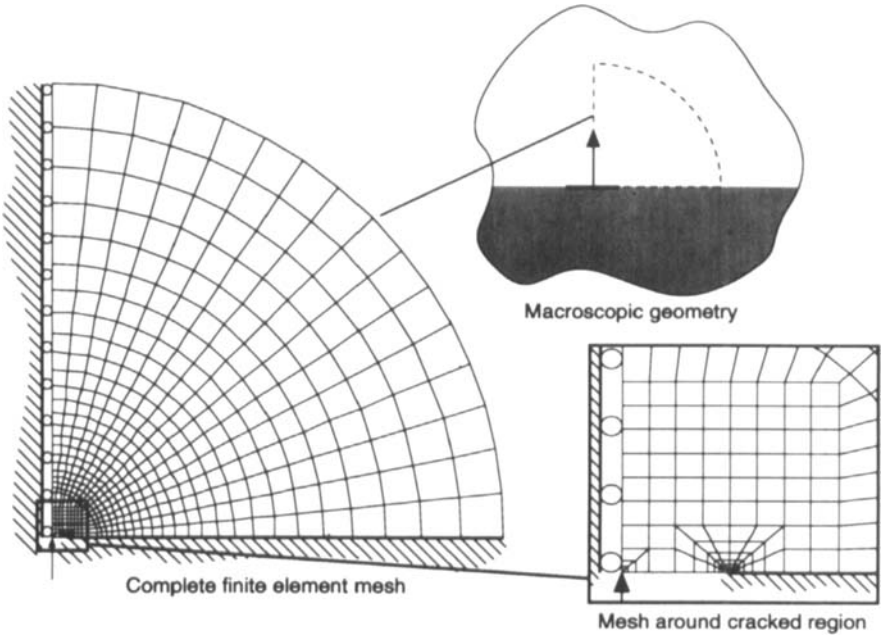

FIGURE 8 From of the point-loaded interface crack model used to assess mesh refinement.

the results are essentially unaffected by the element size. The direct stress perpendicular to the crack and the shear stress parallel to it are shown in Figure 9. Here again it can be seen that with four radial fans in a 90° sector the results are acceptably accurate. Also, the oscillatory nature of the stress field ahead of a bimaterial crack can be seen clearly. From this preliminary study, it was decided to use radial zones of 22.5° and, when calculating energy release rates, to ensure that the smallest element size was one thousandth of the crack length.

Based on the above, the same basic mesh design, seen in Figure 10, has been used in all the subsequent phases of the adhesive joint analyses. It consists of four radial rings in a 90° sector with the smallest element size being dependent on the phase of analysis being carried out. Details are given in the appropriate sections. The mesh is generated automatically using a macro-programme in which both the position of the singularity and the smallest element size are input. It can be seen that three different types of mesh are produced, depending on the crack length being considered. The failure loads have not been applied directly to the model. The results of a three-dimensional study, reported elsewhere,[17] have been used to determine the modified two-dimensional loading corresponding to a unit mode I and mixed mode load. The modified loads are those that reproduce best the adhesive stresses in the region of the joint where the failures occurred. The tensile, shear and moment components of these modified loads (S, P and M, respectively) were evaluated at point O in this earlier work and their variation with crack length for both modes of loading can be seen in Figure 11. In this and some subsequent figures MI and MM refer to the mode I and mixed mode joints, respectively. In the analyses reported in this paper the loads are applied at the positions shown in Figure 10.

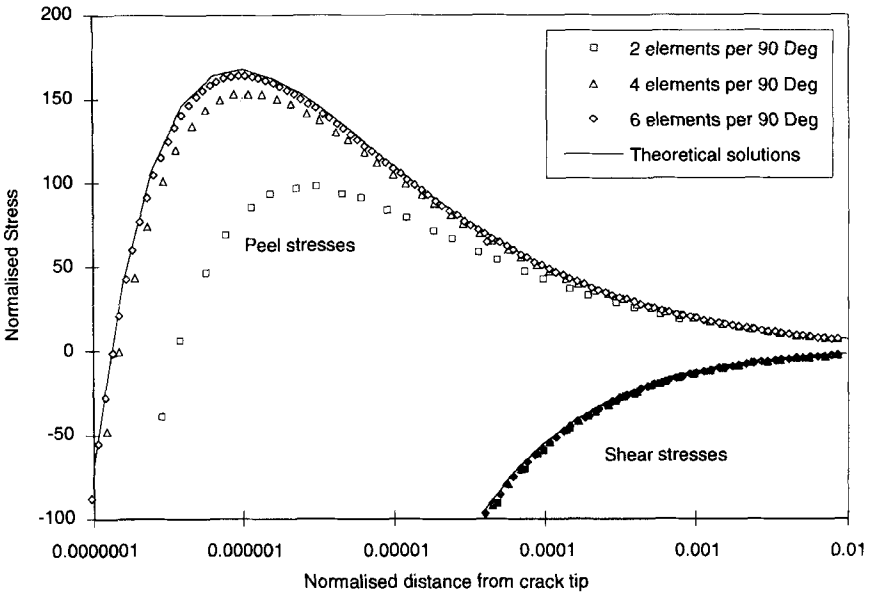

FIGURE 9 Comparison of finite element and analytical shear and peel stresses from the mesh assessment analysis.

The table in that figure gives details of the various loads that are necessary to produce unit tensile, shear and moment loadings at point *O*. Note that for the mixed mode loading there will also be loads at the rear of the joint (see Fig. 1). Figure 11 can then be used to determine how much of each of these tensile, shear and moment loadings is required to produce a unit of actual mode I or mixed mode load. Unless otherwise stated, the elastic material properties used for the epoxy adhesive and the aluminium substrates is given in Table VI.

5. ELASTIC FINITE ELEMENT ANALYSES

5.1 Elastic Analysis for LEFM

A total of ten different crack lengths were considered for both modes of loading (ranging from 0.005 mm to 4 mm) and the smallest element size was set to be 10^{-3} of the crack

TABLE VI
Summary of the elastic material properties used in the finite element analysis

Region	Tensile modulus (N/mm^2)	Poisson's Ratio
Substrate	70000	0.33
Adhesive	2500	0.395

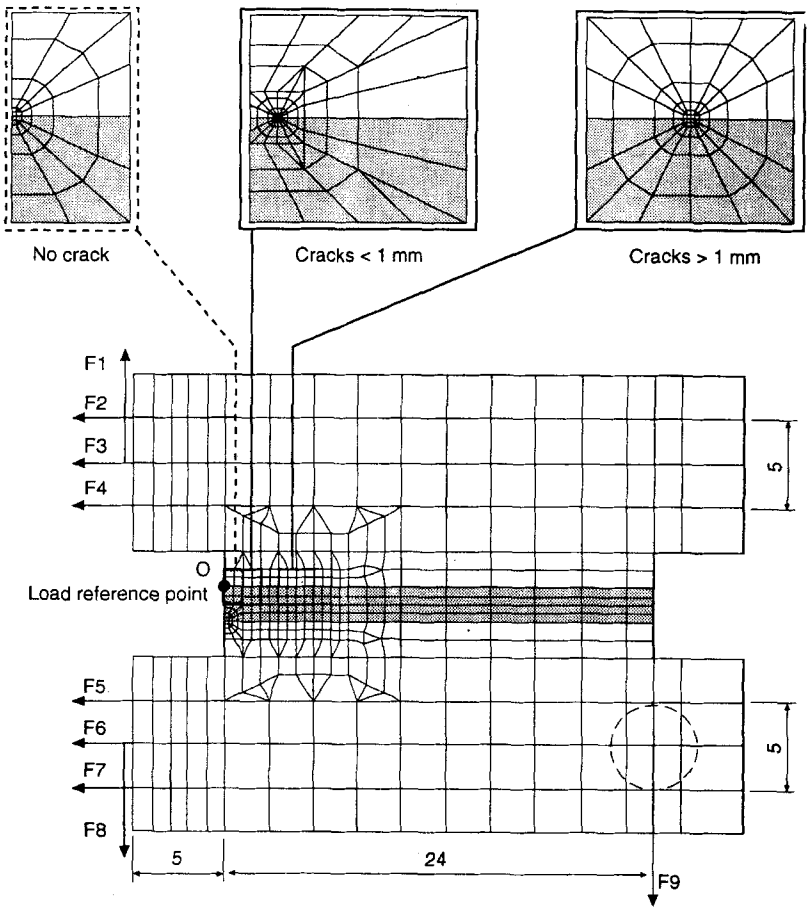

Load Case	F1	F2	F3	F4	F5	F6	F7	F8	F9
Unit Shear - MI	1.0	1.0		-1.0	-1.0		1.0	1.0	
Unit Shear - MM	1.0	1.0		-1.0	-1.72		1.72	1.12	-0.12
Unit Tension - MM		-1.4	1.0	1.4	2.12	-1.0	-2.12		0.68
Unit Moment - MI and MM		-0.2		0.2	0.2		-0.2		

FIGURE 10 Mesh and loading scheme used in the finite element analyses.

length. The energy release rate (G) was found using a virtual crack closure technique. The variation of G with crack length, for a unit applied load, can be seen in Figure 12. The energy released is higher for longer crack lengths and for the mode I loading. Thus, failure at a critical energy release rate would suggest that joints subject to mixed mode loading are stronger than those subject to mode I loads and that the joint strength will decrease with increasing crack length. However, due to the linear nature of the logarithmic plot in Figure 12 it can be seen that G tends to zero in the uncracked configuration (even though there is still a singularity). This implies rapidly increasing failure loads at vanishingly

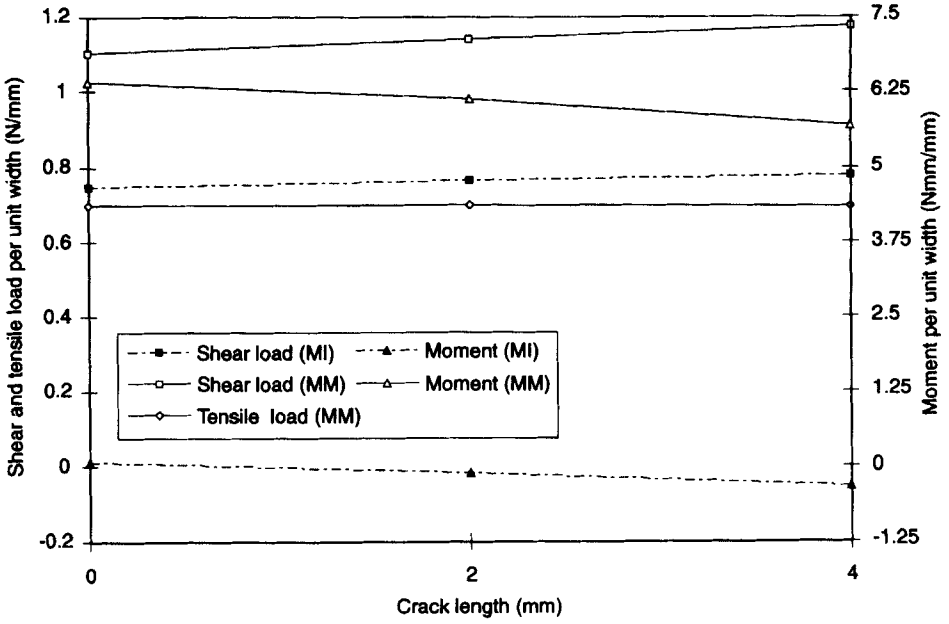

FIGURE 11 Variation with crack length of the modified loads required to simulate a unit applied load.

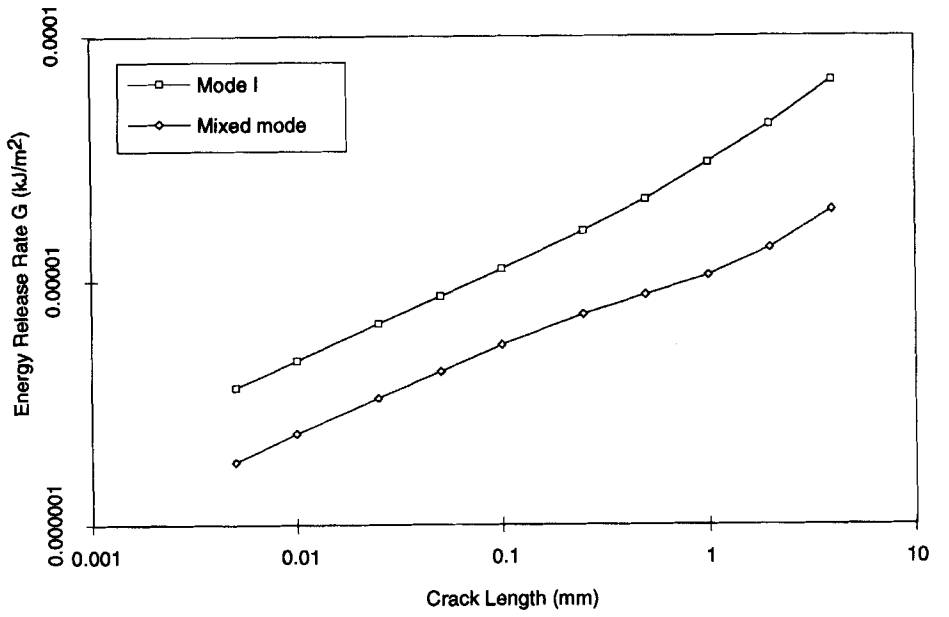

FIGURE 12 Variation of elastic energy release rate with crack length for an applied unit load for both modes of loading.

small crack lengths. This does not happen in practice as failure occurs through plastic deformation and rupture rather than by crack growth at these short crack lengths. An optimum value of G_c is found for the mode I and mixed mode of loading by minimising the error between the predicted and measured failure loads at all data points having crack lengths greater than 0.5 mm. The minimisation was carried out by finding the unit load values of G for each joint tested, by interpolating between the finite element values. A value for G_c is then assumed and the predicted loads for each joint found using this value and the corresponding unit load G value. The error from all data points are then summed (RMS) and the process is repeated until the value of G_c is found that produces the minimum error. This process was carried out automatically on a spreadsheet and gives values of G_c of 0.058 and 0.076 kJ m^{-2} for mode I and mixed mode, respectively. These values are consistent with the data that have been found by other workers in the area.[18] The higher value for the mixed mode joints is probably attributable to the presence of a larger plastic zone. The fit to the experimental data is shown in Figure 13 where it can be seen that at large crack lengths the predicted strengths are good. However, as expected, at short crack lengths serious errors occur in the predicted strengths. This could be overcome by assuming an effective inherent flaw size; however, there is very little physical justification for this. If a common value of G_c of 0.067 kJ m^{-2} were used, then the predicted loads in these figures would each be shifted by about 7%. Thus, the main drawbacks from this approach are the variation of G with mode mixity and the inablility to predict uncracked joint strengths.

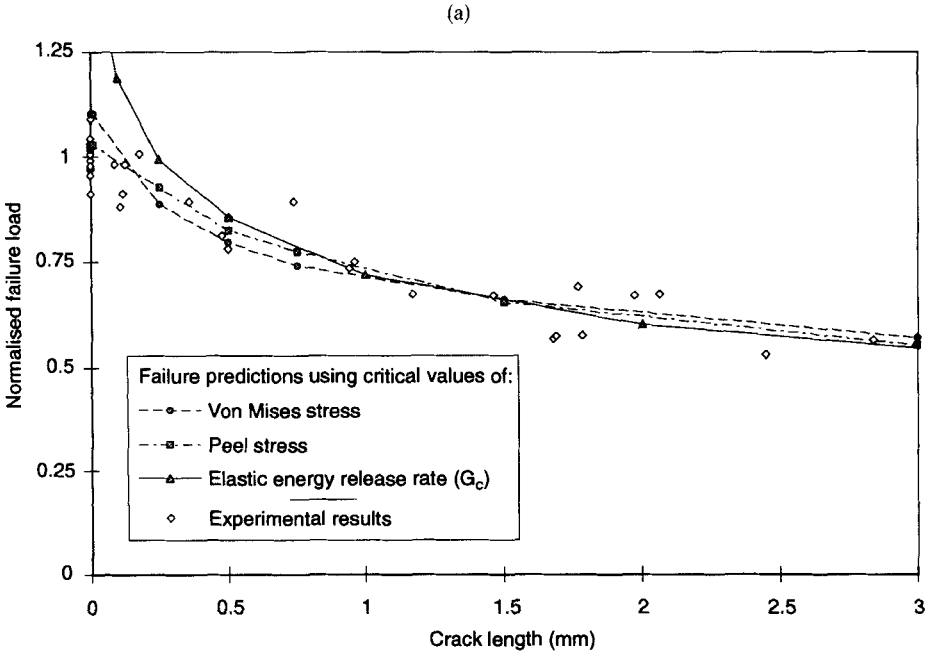

FIGURE 13 A comparison of actual and predicted joint strengths for various crack lengths with various criteria applied in conjunction with linear elastic finite element analyses for a) mode I loading and b) mixed mode loading.

(b)

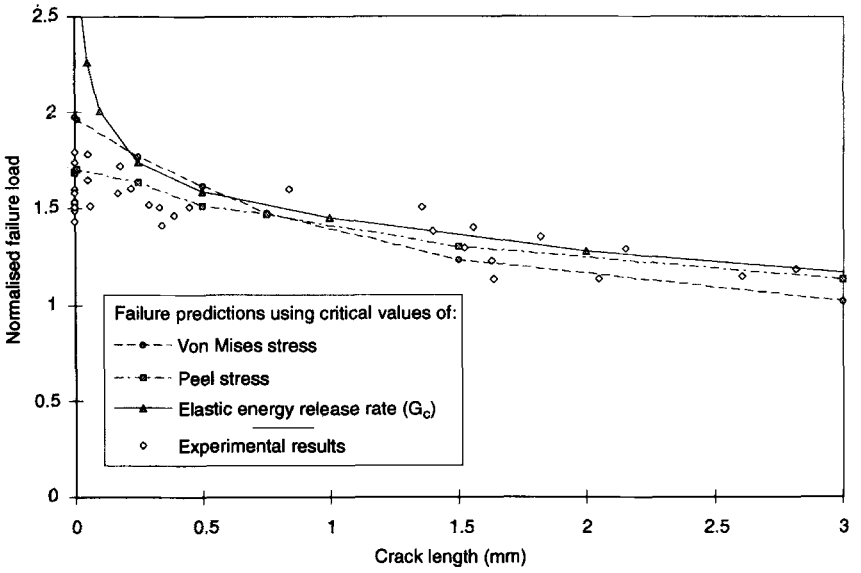

FIGURE 13 *(Continued.)*

5.2 Elastic Analysis For Stress and Strain

Analyses of seven configurations for both modes of loading were carrried out. The seven configurations were uncracked and six other crack lengths ranging from 0.01 to 3 mm. The very small crack length was modelled to investigate the effect of the crack length tending to zero. As we were interested in the detailed stress distribution, a very refined mesh was used with a smallest element size of 0.1 nm. Stresses have been scaled by the appropriate failure loads in order to facilitate comparison between different configurations. The distributions for many components of stress and strain were considered. The direct (peel) stress normal to the interface, the shear stress along the interface and the effective (von Mises) stress have been presented here as these stresses are the most relevant to adhesive joint strength predictions.

The peel stress distributions are shown in Figure 14a for the uncracked and 0.01 and 3 mm cracked configurations under both modes of loading. A number of points can be drawn from these data. The stresses near the singularity vary considerably with crack length and, thus, cannot be used as a unique failure criterion. The strength of the singularity can be found from the gradient of the straight line portions of the data. Evaluating these gradients reveals that both non-cracked configurations have a singularity strength of 0.30, while all the cracked configurations have a strength of 0.49. These values correspond closely to the theoretical values[19] of 0.31 (the non-cracked bi-material singularity strength for the materials and geometry under investigation) and 0.5 (the bounding value of a bimaterial crack). Further, it can be seen that the stresses from the 0.01 mm cracked configuration only follow the singular crack distribution up to about 10 μm, i.e. 0.01 mm, thereafter following the distribution of the uncracked configurations. This implies that the crack tip singularity only dominates up to a distance equal to about

the length of the crack ahead of the singularity. Although the stresses near the singularity appear quite disparate, it can be seen that the stresses appear to converge in the region 0.1 to 1 mm ahead of the singularity. The peel stresses in this region from the same six configurations are shown in Figure 14b. It can be seen that they seem to converge to a common value at about 0.3 mm.

Two parameters are required when using stress as a failure criterion: the value of the stress and the distance from the singular point that this is evaluated, here called the critical distance. Optimum values for these two parameters were obtained by minimising the error between the predicted and actual joint strengths in a manner similar to that used for determining the optimum energy release rate. Using the experimental data from all joints with cracks greater than 0.5 mm appeared to give the best overall correlation between predicted and actual joint strengths. This was done for both the mode I and mixed mode of loading separately and the critical values and distances found are sumarised in Table VII. As can be seen, the critical value and distance found for each mode of loading are almost the same, suggesting that a common value could be used for all modes of loading. A comparison between the predicted and actual joint strengths, using a common critical peel stress of 16.2 MPa at 0.3 mm from the singularity, is shown in Figure 13. The excellent correlation is evident. The main problem with this criterion, however, is that it is rather empirical; the value of 16.2 MPa cannot be related to the bulk adhesive properties and the distance of 0.3 mm is really too far removed from the singularity to define conditions there.

A greater physical significance can be obtained by considering the effective stress distribution and using a critical value of 40.6 MPa, this being the typical ultimate tensile

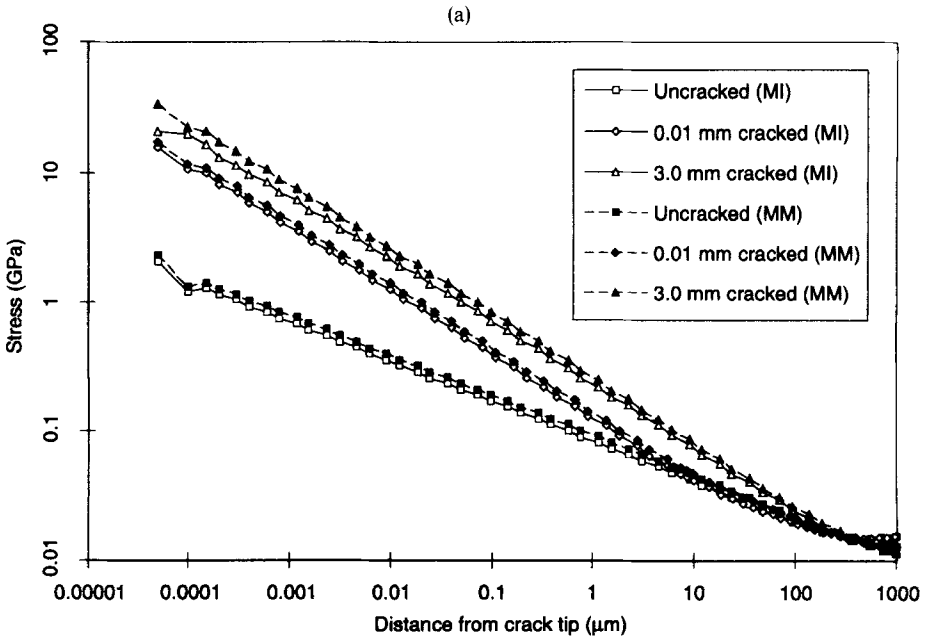

FIGURE 14 Variation of the elastic adhesive peel stresses with distance from the singularity at the measured failure loads: a) near singularity and b) far field.

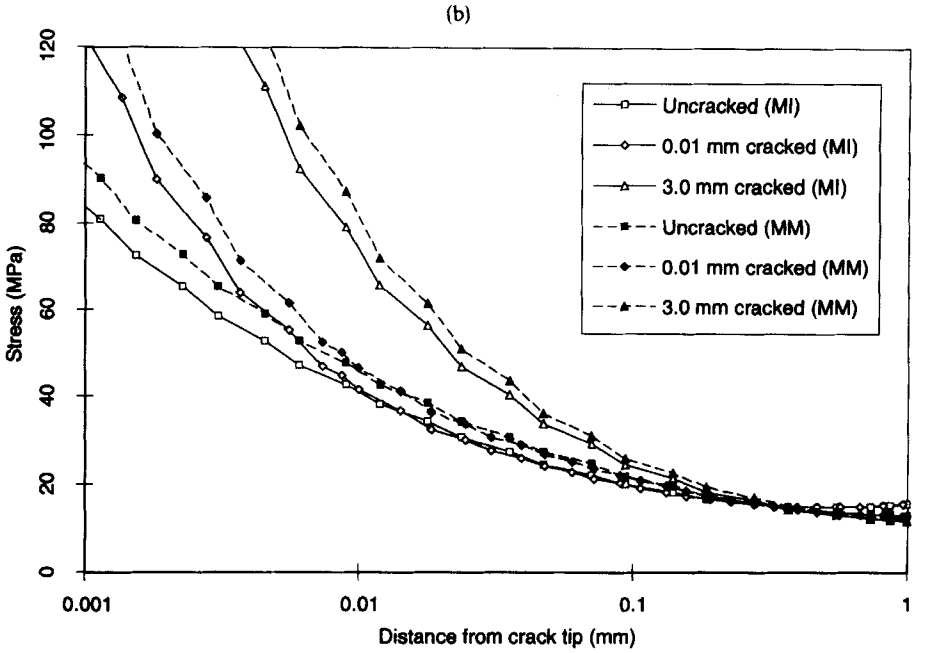

FIGURE 14 *(Continued.)*

TABLE VII
Summary of failure predictions and critical parameters based on elastic stresses at a given distance from the singularity

Mode	Stress Parameter	Critical value (MPa)	Distance (μm)	Cracked RMS Error	Uncracked Error
I	Peel	16.2	300	8.1%	4.1%
Mixed	Peel	16.2	300	7.7%	3.8%
I	Effective	40.6	10.4	8.9%	10.5%
Mixed	Effective	40.6	21.7	12.0%	25.2%

stress of the adhesive for the range of strain rates experienced in this testing. The effective stress distribution for the same six configurations considered above is shown in Figure 15. From this it can be seen that the stresses now no longer converge at a single critical distance. It would appear that the separate modes of loading have different critical distances. Optimisation of this critical distance for each mode of loading substantiates this, giving values of 10.4 and 21.7 μm for mode I and mixed mode loading, respectively. The predicted joint strengths are shown in Figure 13, where it can be seen that the correlation is not as good as that obtained with the peel stresses, particularly in the case of the mixed mode loading, respectively. The predicted joint strengths are shown in Figure 13, where it can be seen that the correlation is not as good as that obtained with

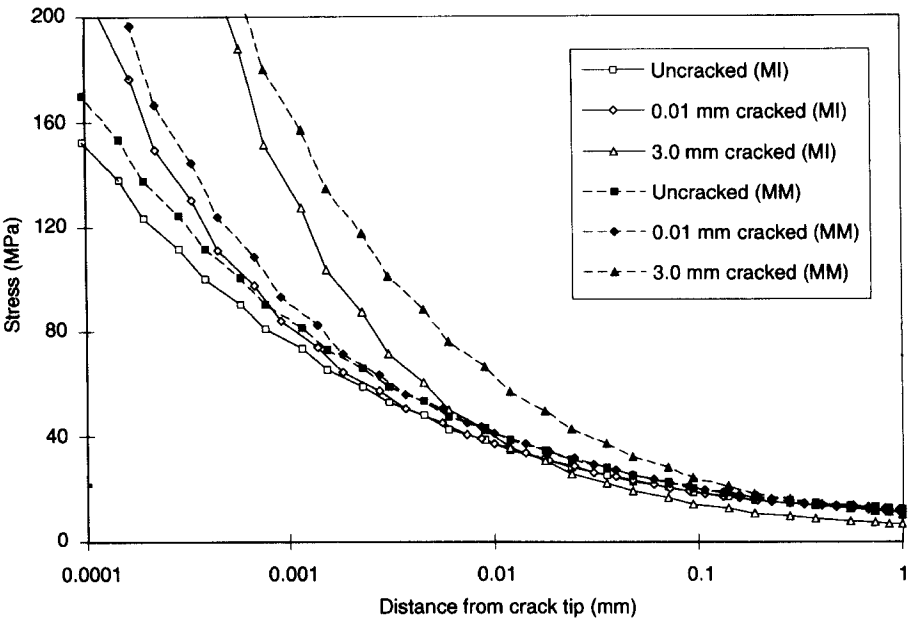

FIGURE 15 Variation of the elastic adhesive effective stresses with distance from the singularity at the measured failure loads.

the peel stresses, particularly in the case of the mixed mode loading. This correlation has been quantified in terms of RMS error, treating the cracked and uncracked joints separately. This is presented in Table VII, where it can be seen that the largest errors occur using the effective stresses with the mixed mode joints. Although physically more meaningful, the fact that the critical distance is a function of the mode mixity restricts the usage of this criterion still further. The critical distance is an indicator of the size of the plastic zone and, as discussed with energy release rates, the mixed mode loaded joints would be expected to develop a larger plastic zone and, hence, the larger critical distance.

Before passing onto the results from non-linear analyses it is interesting to consider the distributions of the shear stresses. These can be seen for all seven configurations of the mode I loaded joints in Figure 16. It can be seen that, unlike all the other component stress distributions, the shape as well as the size of the distribution is highly dependent on the crack length. The uncracked configuration tends to be monotonically increasing with increasing distance from the point of singularity, while the cracked configurations peak and then decrease rapidly. This is due to the oscillatory nature of bi-material cracks. With such behaviour, using shear stresses as a failure criterion would clearly be very difficult to justify.

6. ELASTO-PLASTIC FINITE ELEMENT ANALYSES

The basic mesh configurations discussed in Section 4 were used also for these analyses; however, the size of the element at the singularity was limited to 1 μm. As the yielding of

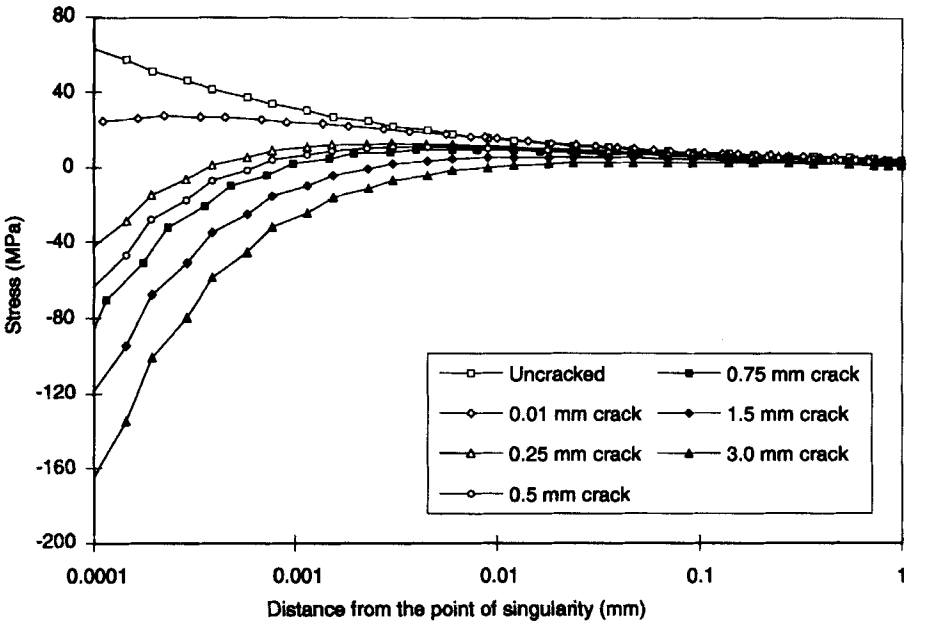

FIGURE 16 Variation of the elastic adhesive shear stresses with distance from the singularity at the measured failure loads.

adhesives is dependent not only on the deviatoric stresses but also on the hydrostatic stresses, it was necessary to code a modified yield criterion for ANSYS, the finite element system that was being used for this work. The following yield function was used, based on the experimental work of Raghava[20] and used by others in the field.

$$\Psi(\sigma) = \frac{(S-1)J_1 + \sqrt{\{[(S-1)J_1]^2 + 12SJ_2\}}}{2S}$$

where

Ψ is the yield function
S is the ratio of the compressive yield stress to the tensile yield stress
$J_{1,2}$ are the first and second stress invariants

It had been intended to investigate how both the energy release rates and the adhesive stress and strain fields were affected by including elasto-plastic behaviour. However, initial studies using crack opening principles, gradually allowing previously-coupled nodes along the interface to separate, showed that, unlike the elastic analyses, the energy release rate obtained varied with the size of the crack length that was allow to open. This introduced problems such as what crack opening distance to use and the way in which this distance should vary with crack length and mode of loading. It was decided that it

would be difficult to obtain consistent and meaningful data. The proposed solution to this problem was the development of the stress-controlled separation analyses which is reported in the next section. In such an approach the length of the process zone is determined automatically. Thus, only work investigating the elasto-plastic stress and strain fields are presented here.

All the configurations considered in the elastic analyses, except for the 0.01 mm crack, were analysed assuming elasto-plastic behaviour of the adhesive. The substrates, manufactured from high-strength aluminium, did not yield during testing. As can be seen from Figure 5, the non-linear adhesive stress-strain curve is significantly dependent on strain rate. It was decided to incorporate a strain rate effect by using a separate material curve for each configuration. This curve would correspond to the average strain rate in the localised plastic zone. As this strain rate is dependent on the constitutive data it was necessary to carry out analyses with stress-strain curves corresponding to two different strain rates. The acutal average strain rates can be found from both analyses and these will almost certainly be at variance from the strain rate data used. An estimate of the appropriate strain rate can then be obtained from a logarithmic interpolation between the assumed and actual strain rates. Thus, two analyses were carried out for each of the twelve configurations considered to determine the appropriate material properties. The average strain rates so obtained are shown in Table VIII. In addition to this, to determine the optimum parameters in any failure criterion, it is necessary to know how the stresses and strains vary with applied load. When the analyses are elastic, this information can be obtained from simple scaling. However, it is not possible to do this and, thus, three analyses were carried out for each configuration, one at the experimental failure load and the others at 10% above and below this value.

Effective stress distributions for all of the mode I configurations are shown in Figure 17. It can be seen that, due to yielding near the singularity, the stresses are initially fairly constant at their appropriate ultimate stress. If a critical stress of 30MPa is assumed (a typical yield stress) then it can be seen that the distance from the point of singularity that this occurs is almost exactly the same size for each configuration. This distance represents the plastic zone size which might form a very reliable (and physically meaningful) failure criterion. Once again, an optimisation procedure has been carried out to determine the best value of the critical distance (or plastic zone size) and the results are presented in Table IX. Comparison with corresponding error data from Table VII shows that this appears to be a better criterion than the elastic effective stress, particularly with the uncracked joint strength predictions. This can be seen in graphical form by comparing the appropriate curves in Figure 14a and 18a. This correlation in the effective stresses away from the point of singularity is interesting, as it shows that the size and

TABLE VIII
Average strain rates (%/min) for mode I and mixed mode configurations

Crack length (mm)	0	0.25	0.50	0.75	1.50	3.00
Mode I	0.175	0.192	0.204	0.242	0.281	0.348
Mixed Mode	0.113	0.127	0.137	0.127	0.144	0.185

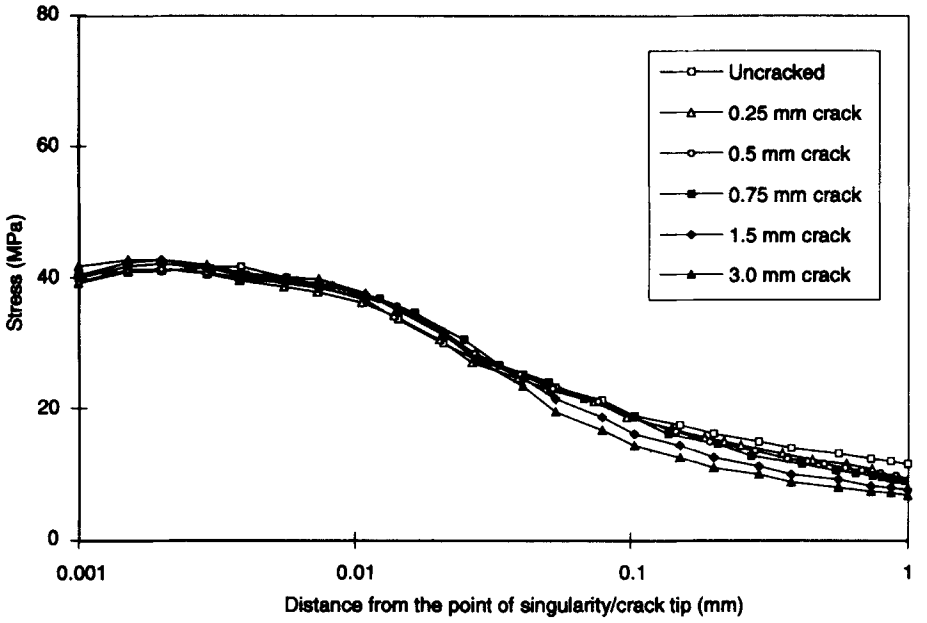

FIGURE 17 Variation of the adhesive effective stresses with distance from the singularity for the elasto-plastic analyses at the measured failure loads.

TABLE IX
Summary of failure predictions and critical parameters based on elasto-plastic stresses at a given distance from the singularity

Mode	Stress Parameter	Critical value (MPa)	Distance (μm)	Cracked Error	Uncracked Error
I	Peel	14.0	500	8.4%	6.2%
Mixed	Peel	14.4	500	7.2%	3.7%
I	Effective	30.0	23	8.1%	2.5%
Mixed	Effective	30.0	47	12.0%	16.3%

shape of the plastic zone is similar in both cracked and uncracked configurations. If failure is governed by an energy balance and the critical energy release rate is dominated by the plastic work, both uncracked and cracked configurations will have similar critical energy release rates. Thus, one energy criterion might apply to both uncracked and cracked states.

The same optimisation procedure, using a critical stress of 30 MPa, has also been carried out for the plastic zone size for the configurations subject to mixed mode loading. the results can be in Table IX and Figure 18b. Although this gives an improvement on the elastic effective stress predictions, the fit to the experimental data is not as good as that obtained with the mode I joints. Also, it should be noted that the distance is larger than in the mode I joints. This indicates that the plastic zone is larger in the mixed mode

specimens and provides a physical basis for the increase in critical energy release rate usually observed in specimens as the loading is changed from mode I to mode II. However, it also means that the criterion is a function of mode mixity and is, thus, more difficult to apply.

Although no distributions for the elasto-plastic peel stresses are shown in this paper, it has been found that, as with the elastic analyses, they coverge to a unique value at a unique distance from the singularity, for all the configurations considered. Optimum values for the critical stress and distance and the corresponding strength predictions have been found in the normal manner and are presented in Table IX and Figure 18, where, by comparison with Table VII and Figure 13, it can be seen that the mixed mode predictions are improved while the mode I predictions are slightly worse.

Although the stresses lose their singular nature in the elasto-plastic analyses, the strains do not. It might be hoped that the strain near the singularity could serve as a failure criterion, being representative of the critical crack tip opening displacement. There was, however, considerable disparity in the strains in the near-singularity region as can be seen in Figure 19, which shows the peel strain distributions for the mixed mode joints. It can be seen that they do converge in the same region that the peel stresses converge but, in fact, they do not provide a better failure criterion here. It is interesting to note that the strength of the singularity now appears to be the same for the uncracked and cracked configurations, unlike the elastic singularities. This suggests that the singularity is now governed more by the material characteristics than by the local geometry.

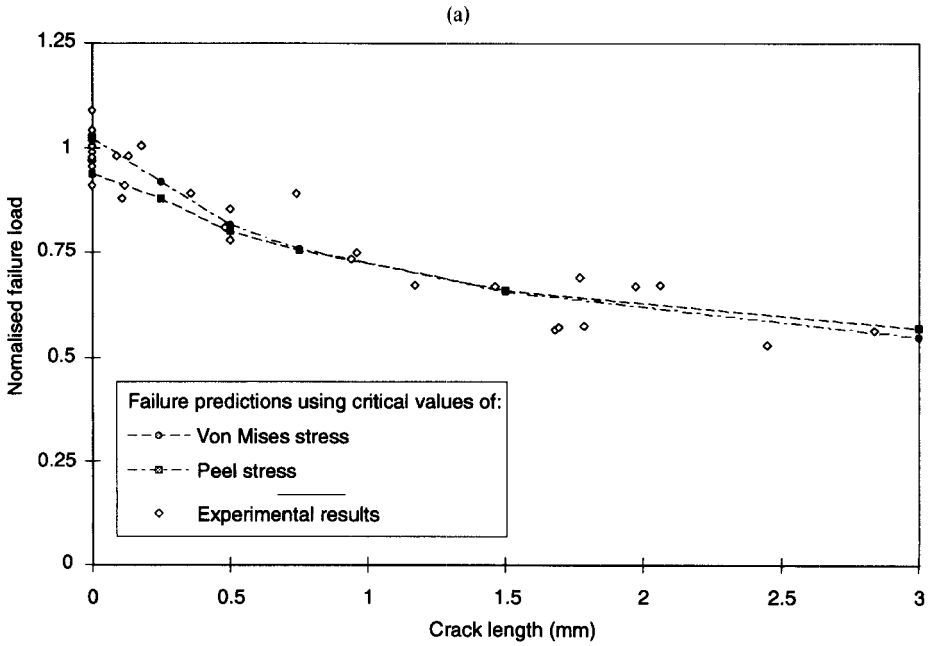

FIGURE 18 A comparison of actual and predicted joint strengths for various crack lengths with various criteria applied in conjunction with elasto-plastic finite element analyses for a) mode I loading and b) mixed mode loading.

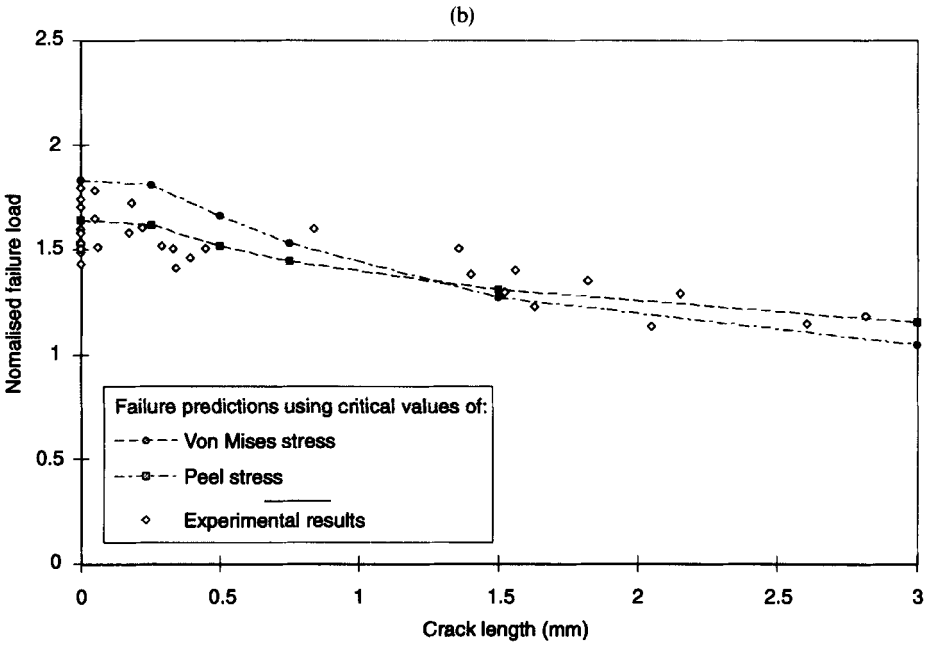

FIGURE 18 *(Continued.)*

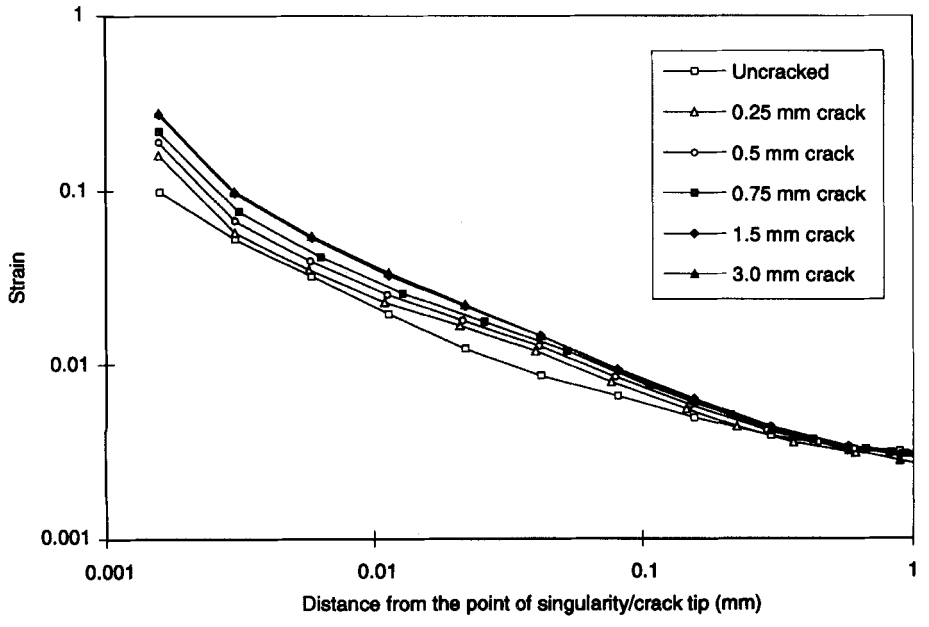

FIGURE 19 Variation of the adhesive peel strains with distance from the singularity for the elasto-plastic analyses at the measured failure loads.

7. STRESS CONTROLLED SEPARATION ANALYSES

This work has been undertaken in an attempt to apply the same energy-based approach to both cracked and uncracked configurations. In this model, it is assumed that all energy-absorbing damage processes that are associated with crack initiation and growth are localised along a line ahead of the singular point. In this respect, it is somewhat akin to the Dugdale model for ductile fracture.[13] In this work, the line process zone lies along the interface between the adhesive and the substrate. The finite element model used for this line zone is shown in Figure 20 and consists of a line of non-linear springs surrounded by an elastic continuum. These non-linear springs are prevented from deforming until the local stress reaches a critical level. Thereafter, they are constrained to deform in a pre-defined manner. In this work, three different spring models have been used: deformation at two different constant stress values (perfectly plastic at 40.6 and 25 MPa) and deformation at a linearly-decreasing level of stress (softening from 40.6 MPa). These are also shown in Figure 20. In these models, the stress of 40.6 MPa was selected as it was the ulimate stress of the adhesive at the average of the strain rates experienced by the adhesive in the joints. The lower value of 25 MPa is somewhat arbitary and has been used to investigate the effect of a larger process zone size. As the load is applied initially, the first and then subsequent springs open. The deformation of the leading spring at the point of the singularity can be used as a failure criterion and is closely related to the crack tip opening displacement used in elasto-plastic fracture mechanics. It can be shown that the energy absorbed by a spring up to failure is the same as the energy required to propagate the process zone, i.e. the energy release rate

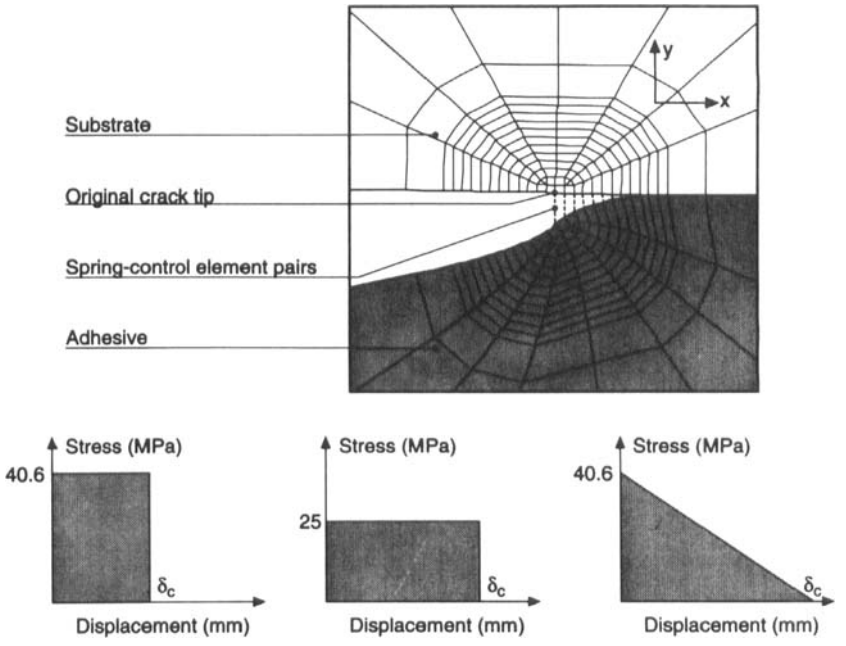

FIGURE 20 The line process zone mesh and spring models used in the stress-contolled separation analyses.

(G). It will be seen that for long crack lengths this approach is equivalent to applying fracture mechanics, whilst for uncracked joints it still predicts finite failure loads, unlike fracture mechanics.

The same configurations considered in the elasto-plastic analyses have also been analysed under stress-controlled separation. The constant stress spring models have been used for both modes of leading, whilst the spring softening model was applied only to the mode I joints. The general procedure for the constant stress models is to leave the critical spring displacement unspecified and to apply a load somewhat in excess of the experimental failure load. Solutions are then obtained, in an incremental manner, for the variation of the first spring displacement with the applied load. This is illustrated in Figure 21 for the mode I loaded joints where springs separate at a constant stress of 25 MPa. These data allow a prediction of a failure load of any configuration for any given critical displacement.

Analyses using the softening springs are more complicated, as it is necessary to specify a critical displacement. With the configurations considered in this work, once this displacement has been exceeded the finite element solution becomes unstable, corresponding to catastropic crack growth. This collapse load is obtained by interpolating between the load increments that straddle it. Thus, in order to assess how the failure load varies with an arbitrary critical displacement the collapse load was determined for three specific critical displacements and an interpolation procedure was used. Here values of 2, 3, and 4μm were used as critical displacements. These were chosen as they covered the range of critical displacements appropriate for this work.

Components of stress and strain in the adhesive adjacent to, and ahead of, the process zone are shown in Figure 22 for the 1.5 mm cracked mode I joint using the model where

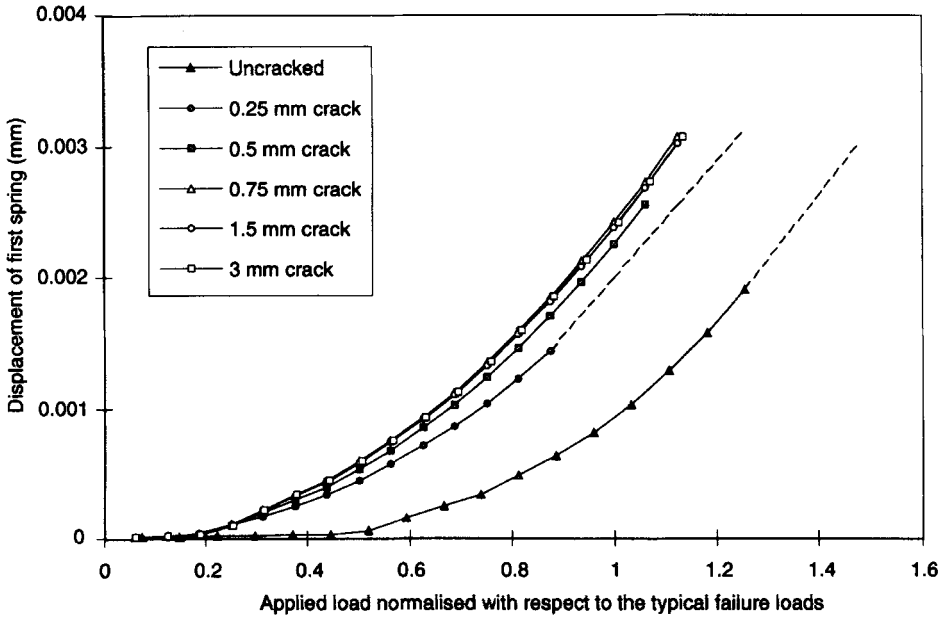

FIGURE 21 The variation of the leading spring displacement with applied mode I loading and a constant separation stress of 25 MPa.

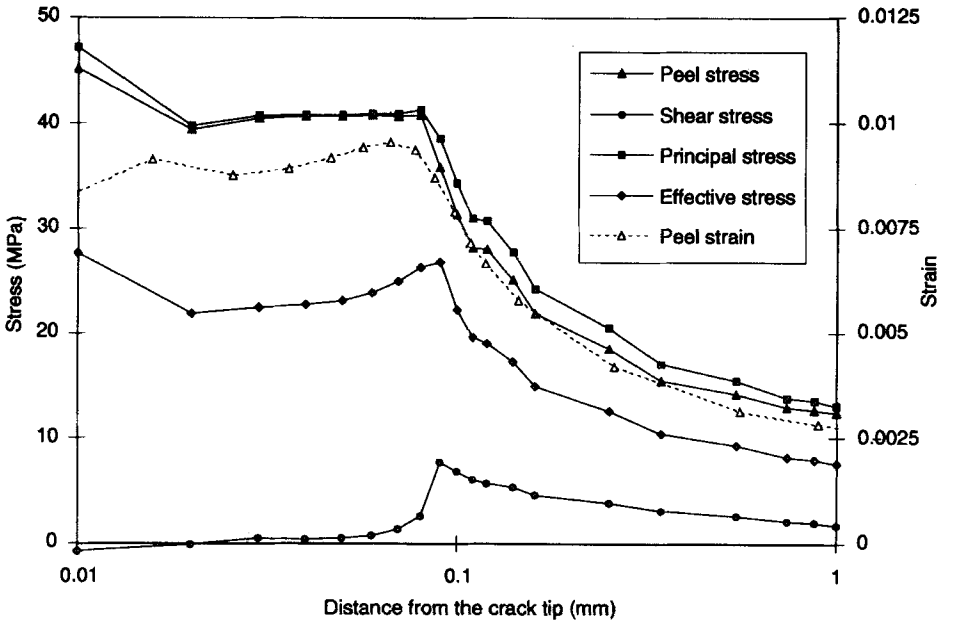

FIGURE 22 Variation of the adhesive stresses and strains with distance from the leading spring for a cracked mode I loaded joint at the measured failure load.

separation occurs at a constant stress of 40.6 MPa and loaded to the experimental failure load. It can be seen that there are no longer any singular fields, even for the strains. The maximum principal stress remains constant at the prescribed value of 40.6 MPa and coincides with the peel stress, showing that, in this region, the adhesive is in a state of uniaxial tension.

Using the information on the variation of failure load with critical spring opening displacement gained from the analyses, it was possible to find the spring displacement that minimises the error between actual and predicted failure load for a given mode of loading. The optimisation scheme used was similar to that used to evaluate the critical parameters in the other failure criteria considered. The values of the critical displacements and the fit to the experimental data is shown in Table X and Fig. 23, respectively.

TABLE X
Summary of failure predictions based on the results from stress controlled separation analyses

Mode	Spring separation stress (MPa)	Critical displacement (mm)	Cracked Error	Uncracked Error	Critical energy (kJ/m^2)
I	40.6(const)	1.38	7.9%	57.6%	0.056
Mixed	40.6(const)	1.81	7.8%	53.2%	0.073
I	25.0(const)	2.26	7.8%	33.7%	0.057
Mixed	25.0(const)	2.95	7.7%	31.9%	0.074
I	40.6(decr)	2.67	7.8%	41.4%	0.054

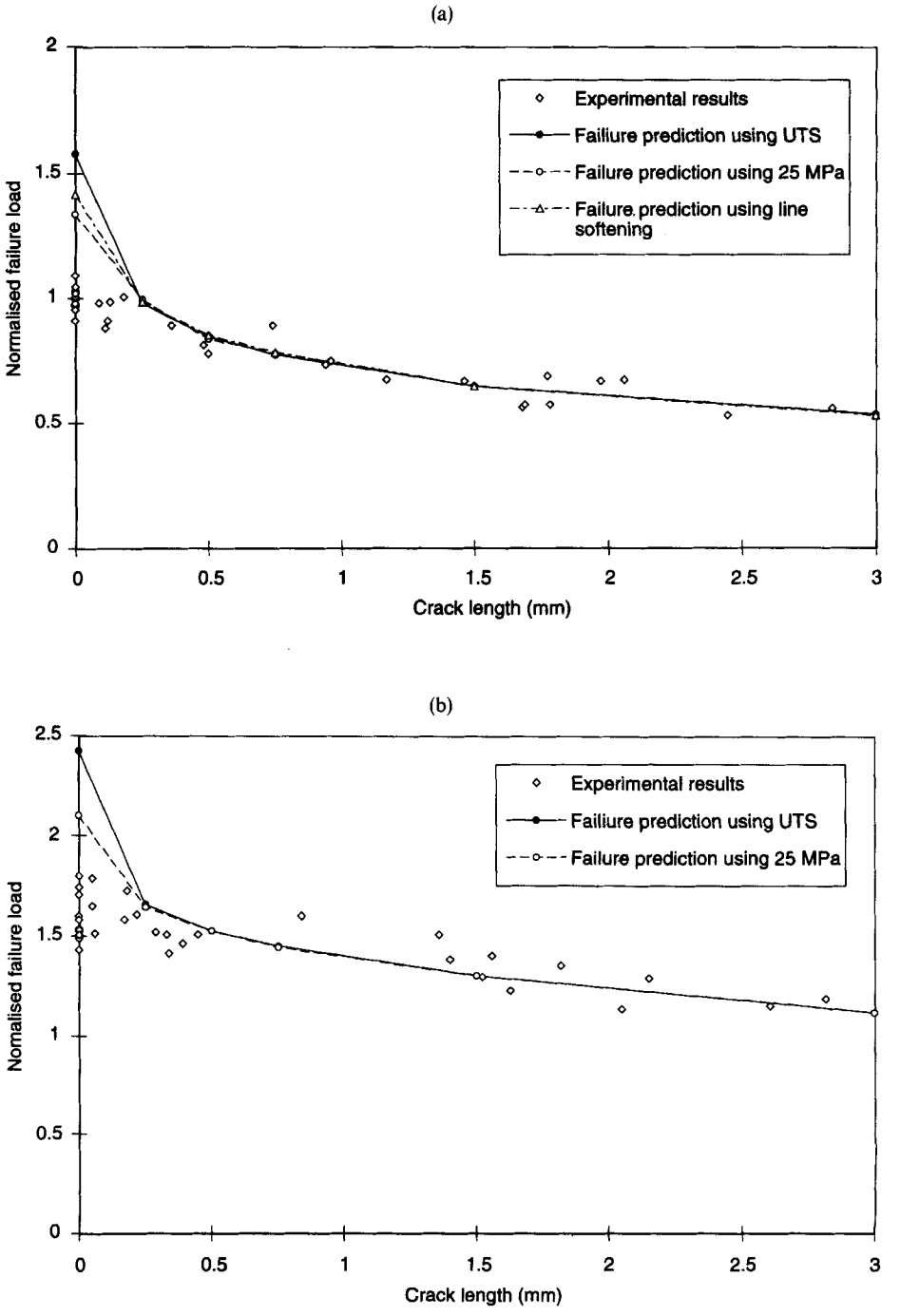

FIGURE 23 A comparison of actual and predicted joint strengths for various crack lengths with various criteria applied in conjunction with stress-controlled separation finite element analyses for a) mode I loading and b) mixed mode loading.

The energy release rate required has also been found from the critical displacement and the separation stress. These are also shown in Table X and, by comparison with Table VII, it can be seen that the stress-controlled separation and the elastic fracture mechanics criteria produce the same critical energy values. The difference between the two criteria is that finite failure loads are predicted with the stress-controlled separation. It can be seen, both from Table X and Figure 23, that having a lower separation stress (and hence a larger process zone) produces a better prediction for the uncracked joints without affecting the accuracy for the cracked configurations. For a given initial separation stress, the linearly-decreasing spring (which is more intuitive) appears to be a better model. The other point to note is that the critical parameters are dependent on mode mixity. This was noted with some of the other criteria and has been attributed to the size of the developed plastic zone. Subsequent work will be directed at modelling stress-controlled separation in an elasto-plastic adhesive and it is anticipated that the critical displacement may then be much less sensitive to the mode mixity.

8. CONCLUSIONS

This paper has presented a programme of experimental and numerical work that enables the relevance of different criteria in predicting the strength of adhesive joints to be compared.

The joint tests have shown that joints loaded in mixed mode are stronger than the same joints in mode I loading. A gradual reduction in failure load from the uncracked to the large crack configuration was found with both modes of loading. The failure initiation was found to be interfacial and the preferred site of failure was found to be within the central half of the joint, lying closer to the interface for mode I loading than for mixed mode loading.

It has been shown that the material property of the adhesive used is rate dependent and that the ultimate strength of the adhesive varies logrithmically with the applied strain rate. An empirical model, for constant strain rate data only, has been found to provide an excellent fit to the experimental tensile data, thus allowing the stress-strain behaviour of the adhesive to be evaluated at an arbitrary rate of straining. This model was subsequently used in conjuction with a stress analysis, allowing the effects of strain rate to be incorporated. Poisson's ratio for the adhesive has been found to be essentially independent of the level of applied longitudinal strain.

A four-point bend test has been used to reconstitute tensile and compressive stress strain curves and, hence, to determine the ratio of the compressive to tensile flow stress. Reasonable correlation between data obtained from tensile and bend tests has established confidence in this new technique. It has been shown that, regardless of the assumed scheme of hardening, the flow stress ratio does not vary significantly over a wide range of straining, justifying the use of a constant value of this ratio in a non-linear stress analysis.

The failure criteria that have been assessed fall into three classes, based on a linear elastic response, an elasto-plastic response and analyses that model the damage that occurs with failure as a line process zone.

Within the first of these classes it was shown that the adhesive peel stress at a specific distance from the singularity provided a unique failure criterion giving excellent joint

strength predictions. The same critical stress and distance parameters were equally applicable to uncracked and cracked joints subject to both mode I and mixed mode loading. The main drawback of this criterion is that it is rather empirical in nature and does not really characterise the near-singularity stress field. The adhesive effective stresses were more physically justifiable as a criterion but yielded critical parameters that were a function of mode mixity. Linear elastic fracture mechanics suffered from the same shortcoming and, of greater concern, did not provide reasonable estimates of uncracked joint strengths.

The incorporation of plastic behaviour for the adhesive changed the stress fields by removing the singularity but produced a stronger strain singularity. The use of peel stresses from these analyses gave no real improvement over the elastic analyses. However, the plastic zone size was found to be remarkably consistent for a given mode of loading and was, thus, useful as a failure criterion. This still suffered, however, from dependency on mode mixity. The strain fields near the the singularity did not show any real correlation between configurations. The use of a crack-opening scheme could not be applied in a consistent way when modelling elasto-plastic material behaviour and, thus, to implement a non-linear, energy-based criterion a scheme based on modelling the process zone was doveloped.

The process zone was modelled as a line of non-linear springs ahead of the singularity. The deformation of these springs could be varied and both perfectly plastic (Dugdale) and softening behaviour were considered. The separation of the initial spring was used as a failure criterion and is similar to the crack tip opening displacement used in ductile fracture mechanics. It was found that the magnitude of separation stress did not affect the accuracy of the predicted cracked joint strengths and that using an initial separation stress somewhat lower than the ultimate stress of the adhesive gave better strength predictions for the uncracked joints. The energy absorbed was shown to be very consistent with the values obtained using linear elastic analyses.

Acknowledgements

The authors would like to express their thanks to Aclan International, SERC and DRA Farnborough, all of whom have provided support and assistance at various stages during the work. Thanks also go to Dr. J. Watts for his help with the XPS analysis.

References

1. ACME Directorate, *Research Priorities in Joining*, London, 1989.
2. G. E. Hale, Working group 8-Design of joints, Design Data Initiative, 1990.
3. J. A Harris and R. D. Adams, *Intl. J. Adhesion and Adhesives*, **4**, 65 (1984).
4. D. A. Bigwood and A. D. Crocombe, *Intl. J.Adhesion and Adhesives*, **10**, 31 (1990).
5. A. D. Crocombe, *Intl. J. Adhesion and Adhesives*, **9**, 145 (1989).
6. H. L.Groth, "Prediction of failure loads of adhesive joints using the singular intensity method", in ASTM STP **945**, 278–284 (1988).
7. T. Hattori, *JSME*, **31**, 718 (1988).
8. A. D. Crocombe, D. A. Bigwood and G. Richardson, *Intl. J. Adhesion and Adhesives*, **10**, 167 (1990).
9. R. A. Geldhill, A. J. Kinloch, S. Yamini, R. J. Young, *Polymer*, **19**, 574 (1978).
10. A. D. Crocombe and R. D. Adams, *J. Adhesion*, **12**, 127 (1981).
11. U. Edlund, *Mechanical Analysis of Adhesive Joints: Models and Computational Methods*, University of Linkoping Studies in Science and Technology. Dissertations, No 291, 1992.

12. G. Laschet and A. Stas, "FE failure prediction of adhesive joints using a simple damage model", *Proc. SAEII*, held at Briotol Univ., UK, 1992, pp. 13/1–13/10.
13. D. Broek, *Elementary Engineering Fracture Mechanics–3rd ed.* (Martinus Nijhoff Publishers, 1982).
14. A. D. Crocombe, G. Richardson and P. A. Smith, *J. Adhesion*, **42**, 209 (1993).
15. H. Eyring, *J. Chem. Phys.*, **4**, 283 (1936).
16. J. F. Loeber and G. C. Sih, *J. Appl. Mechanics*, 240 (1967).
17. G. Richardson, A. D. Crocombe and P. A. Smith, *Int. J. Adhesion and Adhesives*, **13**, 193 (1993).
18. A. J. Kinloch, *Adhesion and Adhesives: Science and Technology* (Chapman and Hall, London and New York, 1987).
19. H. L. Groth, "Singularities at bi-material wedges and interfaces corners", Department of Aeronautical Structures and Materials, The Royal Institute of Technology Stockholm Sweden, Report No 85–2 D1–D12, 1985.
20. R. Raghava, R. M. Caddell and G. S. Y. Yeh, *J. Mater. Sci.* **8**, 225 (1973).